https://doi.org/10.5194/egusphere-2026-3034
Preprint. Discussion started: 11 June 2026

Long-term Strengthening of the CO_2 Sink and Spatiotemporal pCO_2 dynamics in the northern Gulf of Mexico: Insights from a 22-year Satellite-based Machine Learning Reconstruction

Zong-Pei Jiang[1*], Fengqin Chen[1], Wenzhao Liang[2], Kailang Ma[1], Chenfeng Le[1], Yiwen Pan[1], Wei-Jun Cai[3*]

[1]Ocean College, Zhejiang University, Zhoushan, China,

[2]School of Geography and Planning, Sun Yat-sen University, Guangzhou, China

[3]School of Marine Science and Policy, University of Delaware, Newark, DE, USA

Corresponding to: Z.-P. Jiang (zpjiang@zju.edu.cn); W.-J. Cai (wcai@udel.edu)

Abstract

The northern Gulf of Mexico (nGOM) is a river-dominated marginal sea with strong physical-biogeochemical variability. We reconstruct sea surface partial pressure of CO_2 (pCO_2) at 4-km, 8-day resolution from 2003 to 2024 using a satellite-based, season-specific random forest model (independent validation $R^2 = 0.82$, RMSE = 27.6 µatm). The climatological pCO_2 distribution exhibits a sharp coastal-to-offshore gradient: river-influenced coastal waters (SSS < 33) have persistently low pCO_2 with high spatial variability, while offshore waters (SSS > 33) have higher pCO_2 with weaker heterogeneity and lower seasonal amplitude. The nGOM acts as a net CO_2 sink for atmospheric, largely concentrated in the river-influenced plume region due to riverine nutrient-stimulated biological uptake. Seasonal pCO_2 variation is dominantly controlled by temperature but counteracted by spring-summer biological drawdown (reducing pCO_2) and autumn-winter vertical mixing with CO_2-rich deeper water (raising pCO_2). Interannual pCO_2 variability is dominantly affected by year-to-year changes in river discharge and nutrient loading, with higher discharge leading to lower pCO_2 via enhanced biological uptake. On a decadal timescale, sea surface pCO_2 increased at a rate of 0.50 ± 0.20 µatm yr^{-1}, much slower than atmospheric pCO_2 (2.13 ± 0.04 µatm yr^{-1}), leading to a strengthening oceanic CO_2 sink with the sea-to-air flux

https://doi.org/10.5194/egusphere-2026-3034
Preprint. Discussion started: 11 June 2026

becoming more negative at -0.41 ± 0.06 mmol C m^{-2} d^{-1} yr^{-1}. Furthermore, a decreasing frequency of easterly winds has reduced the westward transport of the Mississippi River plume, causing a higher pCO_2 increasing rate on the western Texas-Louisiana shelf.

Plain Language Summary

Using satellite data and a machine-learning model, we produced 22-year (2003-2024) maps of surface ocean CO_2 partial pressure (pCO_2) at 4-km, 8-day resolution for the northern Gulf of Mexico. This dataset helps disentangle how river plumes, seasonal biology, vertical mixing, winds, and climate change control the coastal carbon sink. We find that pCO_2 is low in river-influenced coastal waters because algae consume CO_2 during photosynthesis. Offshore, pCO_2 is higher and more uniform. Seasonally, pCO_2 change follows temperature (high in summer, low in winter), but biological uptake lowers it in spring-summer, while autumn-winter vertical mixing raises pCO_2 by bringing CO_2-rich deep water to the surface. Year-to-year changes in river discharge dominantly drive pCO_2 interannual variability: years with higher river flow bring more nutrients, fueling stronger algal blooms and leading to lower pCO_2. Over 22 years, ocean pCO_2 rose slowly (0.50 µatm yr^{-1}), much slower than atmospheric CO_2 (2.13 µatm yr^{-1}). As a result, the nGOM's CO_2 uptake has increased. Additionally, long-term weakening of easterly winds has reduced the westward spread of the Mississippi River plume, causing pCO_2 on the western Texas-Louisiana shelf to rise faster.

1 Introduction

Marginal seas occupy only ~7 % of the global ocean area, yet they contribute disproportionately to the marine carbon cycle. These regions sustain significantly higher primary productivity than the open ocean due to efficient nutrient delivery from terrestrial runoff and coastal upwelling [*Muller-Karger et al.*, 2005; *Walsh*, 1991]. They overall act as a net sink for atmospheric CO_2 and exhibit high rates of organic carbon burial, thereby playing a critical role in modulating the global carbon budget [*Bauer et al.*, 2013; *Chen and Borges*, 2009; *Dai et al.*, 2022; *Gattuso et al.*, 1998; *Laruelle et al.*, 2018]. Meanwhile, marginal seas are characterized by intense physical-biogeochemical variability, which are shaped by complex hydrodynamic processes (e.g.,

https://doi.org/10.5194/egusphere-2026-3034
Preprint. Discussion started: 11 June 2026

tides, currents, and vertical mixing), elevated nutrient inputs from rivers and anthropogenic sources, high biological productivity, and direct human interventions such as eutrophication and land-use change [*Duan et al.*, 2025; *Roobaert et al.*, 2024]. Under the combined pressures of climate change (e.g., warming, ocean acidification, and altered circulation) and accelerating human activities, understanding how the carbon sink function of marginal seas has evolved and will continue to change is scientifically important and methodologically challenging [*Wei et al.*, 2025].

The northern Gulf of Mexico (nGOM) is a typical river-dominated marginal sea, strongly influenced by the Mississippi-Atchafalaya River System. Large riverine input of nutrients has resulted in eutrophication, leading to one of the world's largest seasonal hypoxic zones and enhanced acidification in bottom waters on the nGOM shelf during summer [*Cai et al.*, 2011; *Jiang et al.*, 2019a, 2024; *Laurent et al.*, 2017; *Rabalais et al.*, 2002]. These characteristics make the nGOM a key area for studying coastal carbon cycling under strong riverine and anthropogenic pressures.

As for the dynamics of sea surface partial pressure of CO_2 (pCO_2) and air-sea CO_2 flux in the nGOM, several in-situ observational studies have revealed their high spatial and temporal variability. Based on 13 cruises conducted between 2003 and 2012, *Huang et al.* [2015] systematically demonstrated a distinct seasonality in CO_2 exchange: the nGOM shelf acted as a net sink of atmospheric CO_2 during spring and early summer, but was neutral or a weak source during midsummer, autumn, and winter. Along the salinity gradient, they identified a clear zonation: the low-salinity zone ($0 \leq S < 17$) was a CO_2 source, the mid-to-high-salinity zone ($17 \leq S < 33$) was a strong CO_2 sink due to enhanced biological uptake fueled by riverine nutrient, and the high-salinity zone ($S \geq 33$) approached equilibrium with the atmosphere. *Kealoha et al.* [2020] analyzed approximately 380,000 Surface Ocean CO_2 Atlas (SOCAT) surface pCO_2 measurements in the Gulf of Mexico from 1996 to 2017 and found that the open and coastal Gulf of Mexico are approximately neutral as an annual source or sink of atmospheric CO_2. In contrast to the long-term increasing sea surface pCO_2 observed in the northwest and southeast open Gulf of Mexico ($\sim 1.70 \pm 0.14$ μatm yr^{-1}), pCO_2 in the Mississippi-influenced central Gulf of Mexico (both coastal and open ocean) remained fairly stable over the same period.

Despite the invaluable insights provided by field observations, the spatial resolution and

https://doi.org/10.5194/egusphere-2026-3034
Preprint. Discussion started: 11 June 2026

temporal coverage of shipboard measurements remain inherently limited, making it difficult to fully resolve the spatiotemporal variability of pCO_2 and air-sea CO_2 flux across the dynamic nGOM. To overcome these limitations and achieve a continuous, satellite remote sensing combined with machine learning has emerged as a powerful alternative. Early efforts to estimate pCO_2 from satellite data in the nGOM include applying empirical regression (root mean square error (RMSE) = 10.66 to 22.94 µatm, R^2 = 0.25 to 0.78) [*Chen et al.*, 2017] and semi-mechanistic approaches (RMSE = 58 µatm) [*Le et al.*, 2019], but they were restricted to summer-only inversions. *Lohrenz et al.* [2018] make a significant advancement by firstly employing a regression tree algorithm, a precursor to machine learning. This model produced the first full-season, multi-year pCO_2 and air-sea CO_2 flux time series for the nGOM during 2006–2010, achieving an RMSE of 28.8 µatm (R^2 = 0.83). Building on this foundation, *Chen et al.* [2019] systematically evaluated seven approaches including multiple linear regression, decision tree, support vector machines, and random forest regression ensemble across the entire GOM. The random forest regression ensemble model, trained with 16 years of *in situ* pCO_2 and satellite data, achieved an overall RMSE of 9.1 µatm (R^2 = 0.95) in open Gulf waters. However, its RMSE increased to 26.1–34.65 µatm in the complex river-dominated nGOM. In addition, the true values of the decadal trend still have large uncertainties in the highly dynamic nGOM due to limited observations and large spatiotemporal variations [*Wu et al.*, 2024].

To better understand the carbon dynamics in the nGOM, this study attempted to develop a season-specific random forest model to reconstruct high-resolution sea surface pCO_2 and air-sea CO_2 flux (4-km, 8 day) over two decades (2003–2024). Our study region focuses specifically on the nGOM shelf (94-88°W, 28-31°N) where riverine influence and spatiotemporal variability are greatest. Our strategy trains dedicated sub-models for spring, summer, autumn, and winter, thereby capturing the unique environmental controls and process regimes that characterize each season in this river-dominated system. This methodological innovation allows us to achieve improved inversion accuracy and generate a continuous, high-resolution pCO_2 product that resolves both seasonal cycles and decadal trends. Based on this dataset, we further investigate the mechanisms driving seasonal pCO_2 variability (e.g., temperature effect vs. biological uptake and vertical mixing) and quantify the long-term evolution of the nGOM's carbon sink, including its response to changing river plume dynamics and atmospheric CO_2 rise.

https://doi.org/10.5194/egusphere-2026-3034
Preprint. Discussion started: 11 June 2026

2 Data and methods

2.1 Data source

Underway measurements of sea surface temperature (SST_{obs}), salinity (SSS_{obs}) and pCO_2 ($pCO_{2,obs}$) in the nGOM were obtained from the SOCAT dataset version 2024 (http://www.socat.info). A total of 205,457 valid measurements were selected within our study region for the period 2003-2024 (Fig. 1a). Riverine discharge and nutrients data were obtained from the United States Geological Survey (https://nwis.waterdata.usgs.gov/) monitoring of the Mississippi River at San Francisville, LA (USGS gage 07373420) and the Atchafalaya River at Melville, LA (USGS gage 07381495). Atmospheric dry-air CO_2 mole fraction (xCO_2) measured at Offshore Corpus Christi, Texas, United States, were downloaded from the Global Monitoring Laboratory Data Viewer (gml.noaa.gov/dv/data/index.php). We then converted xCO_2 to atmospheric pCO_2 ($pCO_{2,air}$) using the empirical formulas of *Zeebe* [2001] for pressure conversion, water-vapor correction, and temperature calibration (Fig. 1b). Sea surface wind speed was obtained from the Cross-Calibrated Multi-Platform vector wind analysis dataset (https://data.remss.com/ccmp/v03.1/). Mixed layer depth (MLD) data were derived from the HYCOM product available at the Ocean Productivity website (https://orca.science.oregonstate.edu/2160.by.4320.8day.hdf.mld125.hycom.php).

Satellite parameters used in this study (Fig. 1c) include sea surface temperature (SST_{sat}), salinity (SSS_{sat}), chlorophyll a ($Chl\text{-}a_{sat}$), and the absorption coefficient of gravel and detritus (a_{dg}). Satellite data for SST_{sat}, $Chl\text{-}a_{sat}$, and a_{dg} were obtained from the Moderate Resolution Imaging Spectroradiometer (MODIS) onboard the Aqua satellite, provided by the National Aeronautics and Space Administration Ocean Color website (https://oceancolor.gsfc.nasa.gov/). Satellite SSS_{sat} was estimated using a local empirical algorithm developed by *Le et al.* [2019] from MODIS-derived terrigenous dissolved organic carbon [*Fichot et al.*, 2014].

2.2 Model development, validation, and application

2.2.1 Data matching for model training and validation

https://doi.org/10.5194/egusphere-2026-3034
Preprint. Discussion started: 11 June 2026

To build a robust empirical relationship between satellite-derived environmental variables and sea surface pCO_2, we first matched the *in situ* $pCO_{2,obs}$ measurements with collocated satellite data and atmospheric $pCO_{2,air}$. Specifically, for each $pCO_{2,obs}$ observation, we extracted the corresponding satellite-derived SST_{sat}, Chl-a_{sat}, a_{dg}, and SSS_{sat} at the same location and date (the median value of a 3×3 pixel box centered on each sampling point). We also included the contemporaneous atmospheric $pCO_{2,air}$ linearly interpolated to the observation time. This procedure produced a set of matched arrays, each containing one $pCO_{2,obs}$ value together with its associated SST_{sat}, Chl-a_{sat}, a_{dg}, SSS_{sat}, and $pCO_{2,air}$ (Fig. 1d). After excluding extreme $pCO_{2,obs}$ values < 145 µatm or > 550 µatm, we obtained 18,648 valid matched samples covering 2003–2024 (Table S1). It is worth noting that our reconstruction did not include the extreme high pCO_2 (up to 2000 µatm when $S < 5$) in the river channel caused by terrestrial organic matter decomposition [*Huang et al.*, 2015]. Due to rapid mixing of river and seawater, the area affected by this high-pCO_2 freshwater is very small relative to the total study region, and thus does not affect the overall analysis or flux estimates in our study.

2.2.2 Model training and validation

The matched dataset was randomly split into three subsets: 52.5% for training, 17.5% for internal validation (hyperparameter tuning), and 30% for external independent validation. The independent validation set was held out throughout the entire model development process and was used only once to evaluate the final model's generalizability. We adopted a random forest regression algorithm because of its ability to capture nonlinear interactions and its robustness to overfitting [*Chen et al.*, 2019]. During model development, we compared two training strategies: 1) a full-season model: all samples from all seasons were pooled together to train a single random forest model; 2) a season-specific model: the training samples were separated by season (spring: March–May; summer: June–August; autumn: September–November; winter: December–February), and four independent sub-models were trained. The latter integrated framework allows us to capture the distinct environmental controls of each season while maintaining a consistent methodological structure. Model performance was quantified using the coefficient of determination (R^2), root mean square error (RMSE), mean absolute error (MAE), mean relative error (MRE), and mean ratio (MR). The season-specific approach consistently outperformed the full-season model, yielding an overall

https://doi.org/10.5194/egusphere-2026-3034
Preprint. Discussion started: 11 June 2026

lower RMSE (27.6 vs. 31.4 µatm) and higher R^2 (0.81 vs. 0.77) on the independent validation sets (Table S2). Consequently, we selected the season-specific random forest model as our final configuration.

2.2.3 Model application to generate gridded pCO_2 products

Once trained and validated, the season-specific random forest model was applied to produce a continuous, high-resolution pCO_2 product over the nGOM for 2003–2024. In this application step, the satellite remote sensing data served as the spatial and temporal anchor (Fig. 1e). For each 8-day composite and each 4 km grid cell, we extracted the corresponding satellite-derived SST_{sat}, Chl-a_{sat}, a_{dg}, and SSS_{sat}. We then matched these gridded satellite data with the contemporaneous $pCO_{2,air}$ to form gridded inputs (one array per grid cell and time step). These gridded inputs were then fed into the season-specific random forest model to generate an output gridded field of sea surface pCO_2 ($pCO_{2,\,model}$) for each 8-day period at 4 km spatial resolution (Fig. 1g).

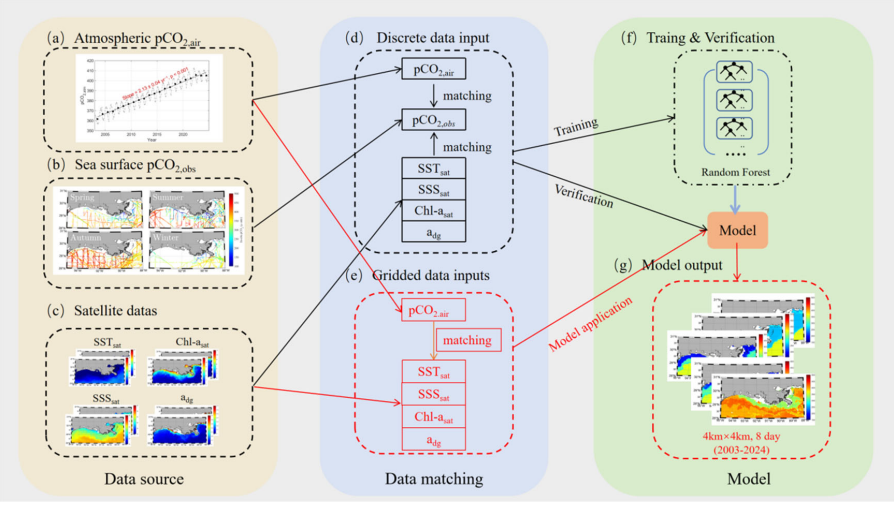

Figure 1. Framework of the seasonal-specific random forest model. Data source includes: (a) long-term trend of atmospheric $pCO_{2,air}$; (b) sea surface $pCO_{2,obs}$ from underway measurements; (c) satellite data of sea surface temperature (SST_{sat}), chlorophyll a (Chl-a_{sat}), the absorption coefficient of gravel and detritus (a_{dg}), and salinity (SSS_{sat}). Matched data were used for (d, f) model training and validation, as well as for (e, g) model application to generate gridded fields of sea surface pCO_2 ($pCO_{2,\,model}$) at 8-day temporal resolution and 4 km spatial resolution. See Section 2.2 for details.

https://doi.org/10.5194/egusphere-2026-3034
Preprint. Discussion started: 11 June 2026

2.3 Calculations

To investigate the driving mechanisms of pCO_2 variability, we quantified the thermal and non-thermal effects on pCO_2 using a temperature sensitivity coefficient of 0.0423°C^{-1} [*Takahashi et al.*, 1993] .

$$T pCO_2 = pCO_{2,mean} * \exp\left(0.0423 * (SST - SST_{mean})\right)$$

$$N pCO_2 = pCO_2 * \exp\left(0.0423 * (SST_{mean} - SST)\right)$$

where TpCO_2 is the thermally-driven pCO_2 changes resulting from SST fluctuation relative to the mean sea surface temperature (SST_{mean}) and the mean pCO_2 ($pCO_{2,mean}$), while temperature-normalized NpCO_2 reflects the non-thermal effects on pCO_2 due to physical mixing and biogeochemical processes.

The sea-to-air CO_2 flux (F_{CO2}, mmol C m^{-2} d^{-1}) was calculated as:

$$F_{CO2} = k\,\alpha\,\Delta pCO_2 = k\,\alpha\left(pCO_{2,sw} - pCO_{2,air}\right)$$

where k is the gas transfer velocity estimated from wind speed using the parameterization of *Wanninkhof* [2014], α is the gas solubility of CO_2 as a function of seawater temperature and salinity [*Weiss*, 1974], and ΔpCO_2 is the pCO_2 difference between the seawater ($pCO_{2,sw}$) and the atmosphere ($pCO_{2,air}$).

3 Results and Discussion

3.1 Performance of the season-specific random forest model

We evaluated the performance of the season-specific random forest model by comparing the reconstructed $pCO_{2,model}$ against the collocated in situ observations ($pCO_{2,obs}$) for the training, internal validation, and external independent validation datasets. The evaluation results demonstrated that the model exhibited good performance and robustness across all datasets (Fig. 2). The training dataset achieved an overall R^2 of 0.97 and an RMSE of 11.51 μatm, indicating strong learning ability (Fig. 2a). The internal validation dataset yielded an R^2 of 0.81 and an RMSE of 28.53 μatm (Fig. 2b). For the external independent validation, the four seasonal sub-models showed comparable R^2 values ranging from 0.70 to 0.82. Owing to the high freshwater and nutrient inputs from river discharge, which drive strong plume dynamics and high biological productivity, pCO_2 in spring and summer exhibits greater spatiotemporal variability [*Huang et al.*, 2015]. Consequently,

https://doi.org/10.5194/egusphere-2026-3034
Preprint. Discussion started: 11 June 2026

the RMSE of the spring and summer sub-models (32.4 and 34.4 µatm) was slightly higher than that of the autumn and winter sub-models (22.1 and 22.3 µatm). Overall, the external independent validation set demonstrated the model's good generalization ability and reliability, with a combined R^2 of 0.82 and an RMSE of 27.60 µatm (Fig. 2c). Additional validation on individual cruise further confirmed that the model successfully captures the spatiotemporal variability of pCO_2 in the nGOM (Fig. S1). The reconstruction provides a solid basis for the subsequent analysis of seasonal to decadal variability of pCO_2 and air-sea CO_2 flux in the highly dynamic nGOM and their underlying mechanisms.

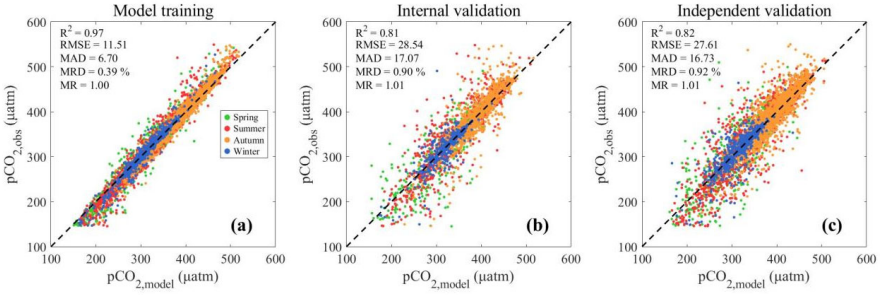

Figure 2. Comparison between in situ observed sea surface pCO_2 ($pCO_{2,obs}$) and reconstructed pCO_2 from the season-specific random forest model ($pCO_{2,model}$) for (a) the training dataset, (b) the internal validation dataset, and (c) the external independent validation dataset. Points are color-coded by season (spring, summer, autumn, winter). Also shown are the coefficient of determination (R^2), root mean square error (RMSE), mean absolute error (MAE), mean relative deviation (MRD) and mean relative error (MR).

3.2 Climatological distribution of sea surface pCO_2

To characterize the overall pCO_2 distribution, we computed the climatological mean pCO_2 fields based on the high-resolution time-series output from our season-specific random forest model. The long-term pCO_2 change rate (estimated from regional and monthly averaged pCO_2; see Section 3.4) was used to remove sampling-year biases, yielding a climatological mean normalized to a single reference year 2013 (Fig. 3). The climatological annual mean pCO_2 (Fig. 3a), its annual amplitude (Fig. 3b), and the seasonal climatological fields (Fig. 3c–f) all exhibit a clear contrast between the river-influenced coastal region (approximately within the 33 isohaline) and the outer shelf (high-salinity offshore waters).

A clear coastal-to-offshore gradient exists, with lower pCO_2, stronger spatial heterogeneity,

https://doi.org/10.5194/egusphere-2026-3034
Preprint. Discussion started: 11 June 2026

and higher annual amplitude in the coastal region compared to the outer shelf (Fig. 3). The annual mean of climatological pCO_2 in coastal water (310.9 µatm for salinity < 33) is generally below the atmospheric level (383.0 µatm in reference year 2013), except in some nearshore areas adjacent to the Mississippi and Atchafalaya estuaries. The lowest pCO_2 values and the strongest spatial heterogeneity occur in the plume region during spring and summer (Fig. 3c, d). In contrast, the high-salinity Gulf waters show a higher annual mean of climatological pCO_2 (374.3 µatm for salinity > 33), especially in summer and autumn (Fig. 3d, e), with a much more uniform distribution. Moreover, the annual amplitude of pCO_2 on the outer shelf (mean value of 88.4 µatm) is smaller than that in the dynamic coastal region (mean value of 133.1 µatm, Fig. 3b).

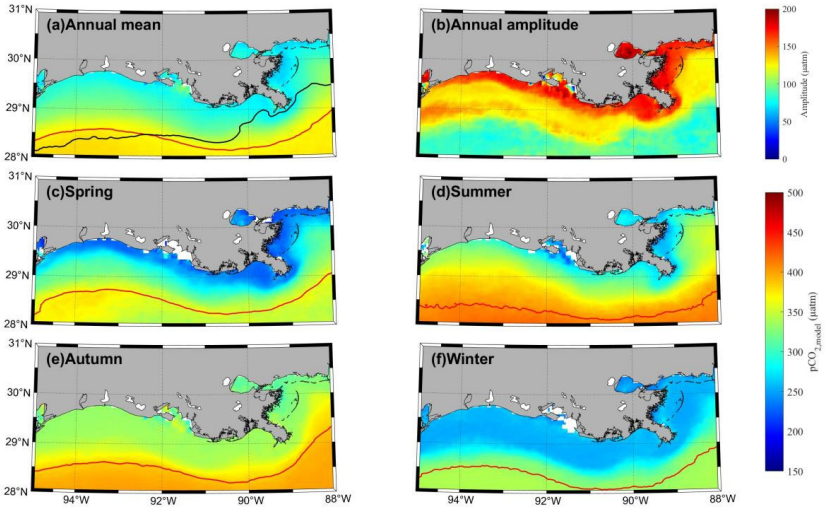

Figure 3. Climatological (a) annual mean (average of monthly means) and (b) annual amplitude (maximum minus minimum monthly mean) of sea surface pCO_2 estimated from the season-specific random forest model normalized to the reference year 2013. Seasonal climatological fields of pCO_2 in (c) spring, (d) summer, (e) autumn, and (f) winter. The black dashed line in panel (a) marks the 50 m isobath, and the red solid lines mark the 33 isohalines. Note that the color bar in panel (b) differs from those in the other panels.

3.3 Seasonal to interannual variability of pCO_2

3.3.1 Seasonal patterns

In addition to the spatial differences described in Section 3.2, the climatological regional

https://doi.org/10.5194/egusphere-2026-3034
Preprint. Discussion started: 11 June 2026

monthly averages of key environmental variables reveal strong and coherent seasonal variations in the nGOM (Fig. 4, Table S3). Sea surface temperature (Fig. 4a) exhibits a pronounced seasonal cycle, rising steadily from a winter minimum of 18.7 °C to a summer maximum of 30.7 °C. Mississippi River discharge and total nitrogen (TN) load are highly correlated, both peaking in May and reaching their annual minima in autumn (Fig. 4c). The elevated riverine freshwater input results in lower salinity during spring and summer compared to autumn and winter (Fig. 4b, c). In response to the riverine nutrient input, chlorophyll-a (Chl-a) begins to increase in spring (Fig. 4d), but the biological uptake lags behind the nutrient supply with Chl-a peaking in July, consistent with previous observations [*Turner et al.*, 2006]. The elevated vertical export of particulate organic matter from high spring-summer productivity and its subsequent decomposition at depth, together with strong stratification, drive the well-known summer bottom-water hypoxia and acidification on the nGOM shelf [*Cai et al.*, 2011; *Jiang et al.*, 2019a; *Rabalais et al.*, 2002].

Atmospheric $pCO_{2,air}$ shows a clear seasonal pattern, with a summer minimum of 378.9 µatm and a winter maximum of 391.7 µatm (Fig. 4e). In contrast, sea surface $pCO_{2,model}$ (Fig. 4f) reaches its highest value in September (387.9 µatm) and its lowest value in January (283.8 µatm), with an annual amplitude (104.1 µatm) substantially larger than that of $pCO_{2,air}$ (12.8 µatm). This seasonality of sea surface pCO_2 is consistent with previous in situ observations [*Huang et al.*, 2015]. Consequently, the seasonal variability of the air-sea pCO_2 difference (ΔpCO_2, Fig. 4g) is largely controlled by that of $pCO_{2,model}$. Except in September, ΔpCO_2 is negative (sea surface pCO_2 below atmospheric level) throughout the year, indicating persistent oceanic CO_2 uptake in the nGOM, which is largely concentrated in the low-pCO_2 river-influenced coastal region (Fig. 3).

The seasonal trend of air-sea CO_2 flux (F_{CO2}, Fig. 4i) is synchronized with ΔpCO_2, but the magnitude of F_{CO2} is also regulated by wind speed (Fig. 4h). In spring and winter, highly negative ΔpCO_2 combined with high wind speeds (up to 5.7 m s^{-1}) produces the strongest oceanic CO_2 uptake (up to -37.1 mmol C m^{-2} d^{-1}). In summer, ΔpCO_2 is close to zero or slightly positive and wind speed remains low (3.6 to 4.3 m s^{-1}), leading to weak oceanic uptake or slight release (-3.1 to 1.5 mmol C m^{-2} d^{-1}). On an annual climatological basis, the entire nGOM acts as a net sink for atmospheric CO_2, with a mean flux of -9.97 mmol C m^{-2} d^{-1} (or -3.63 mol C m^{-2} yr^{-1}). When separated into coastal (SSS < 33) and offshore waters (SSS > 33), both sub-regions exhibit similar seasonal trends in F_{CO2}, but their flux magnitudes differ significantly (Fig. S3). The high-salinity,

https://doi.org/10.5194/egusphere-2026-3034
Preprint. Discussion started: 11 June 2026

low-Chl-a offshore water acts as a weak CO_2 source during summer and autumn, transitioning to a sink in winter and spring. On an annual basis, the offshore water is a weak net sink, with an annual flux of -0.15 mol C m^{-2} yr^{-1}. In contrast, coastal water maintains pCO_2 below atmospheric levels throughout the entire year, resulting in continuous CO_2 uptake from the atmosphere and an annual net CO_2 sink of -3.48 mol C m^{-2} yr^{-1}. Therefore, the CO_2 uptake in the nGOM is predominantly contributed by the river-influenced coastal water.

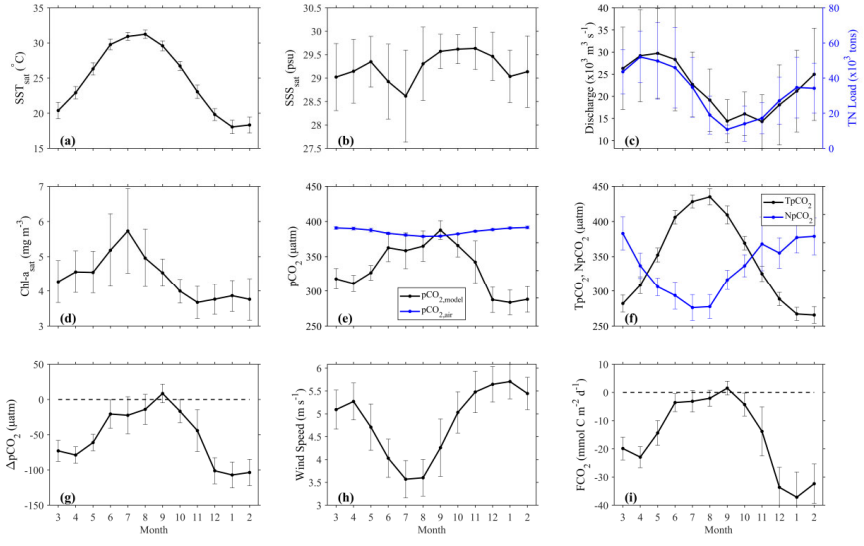

Figure 4. Seasonal variations of key surface water variables in the northern Gulf of Mexico: (a) satellite-derived sea surface temperature (SST_{sat}); (b) satellite-derived salinity (SSS_{sat}); (c) Mississippi River discharge and total nitrogen (TN) load; (d) satellite-derived chlorophyll a (Chl-a_{sat}); (e) sea surface pCO_2 from the season-specific random forest model ($pCO_{2,model}$) and atmospheric pCO_2 ($pCO_{2,air}$); (f) thermally driven change in sea surface pCO_2 ($TpCO_2$) and non-thermal effect on pCO_2 ($NpCO_2$); (g) air-sea pCO_2 difference (ΔpCO_2, seawater minus atmosphere); (h) wind speed; (i) sea-to-air CO_2 flux (F_{CO2}), where negative values refer to oceanic CO_2 uptake. Solid points represent the climatological regional monthly averages, with error bars indicating the standard deviation arising from spatial heterogeneity. Dashed lines in panels (g) and (i) mark the zero line (pCO_2 equilibrium and zero flux, respectively).

3.3.2 Controls on seasonal and inter-annual variability of sea surface pCO_2

The seasonal cycle of sea surface pCO_2 generally follows that of SST (Fig. 4): warmer waters

https://doi.org/10.5194/egusphere-2026-3034
Preprint. Discussion started: 11 June 2026

increase pCO_2 by reducing CO_2 solubility, while cooler waters have the opposite effect. The thermally driven changes in pCO_2 ($TpCO_2$) exhibits a high seasonal amplitude of 178.5 µatm (Fig. 4f), whereas the non-thermal component ($NpCO_2$) varies in opposite phase, with a lower amplitude of 106.7 µatm (Fig. 4f). Thus, the pCO_2 seasonality is dominantly controlled by temperature, partially counteracted by non-thermal effects. In the following text, we further examine the dominant non-thermal mechanisms in different seasons.

Biological uptake in spring and summer: The spring-summer climatology demonstrates that the spatial distribution of pCO_2 and $NpCO_2$ is highly synchronous with the evolution of the plume trajectory (Fig. 5), which is modulated by river discharge and wind patterns [*Huang et al.*, 2013; *Schiller et al.*, 2011; *Walker*, 1996; *Zhang et al.*, 2012b]. Elevated chlorophyll-a in plume region clearly shows the significant stimulatory effect of riverine nutrient inputs on phytoplankton biomass (Fig. 5a-f). The resulting photosynthetic carbon fixation strongly consumes dissolved CO_2 in surface waters, leading to a pronounced decrease in both pCO_2 and the $NpCO_2$ (Fig. 5g-l). This biological drawdown is most evident in the mid-salinity plume region (SSS 15–20), consistent with previous shipboard observations [*Jiang et al.*, 2019b]. Laboratory incubation experiments have demonstrated the occurrence of an “optimal growth region” at intermediate salinities, depending on the balance between enhancing nutrient limitation and reducing light limitation with increasing salinity in estuarine environments [*Jiang et al.*, 2021].

https://doi.org/10.5194/egusphere-2026-3034
Preprint. Discussion started: 11 June 2026

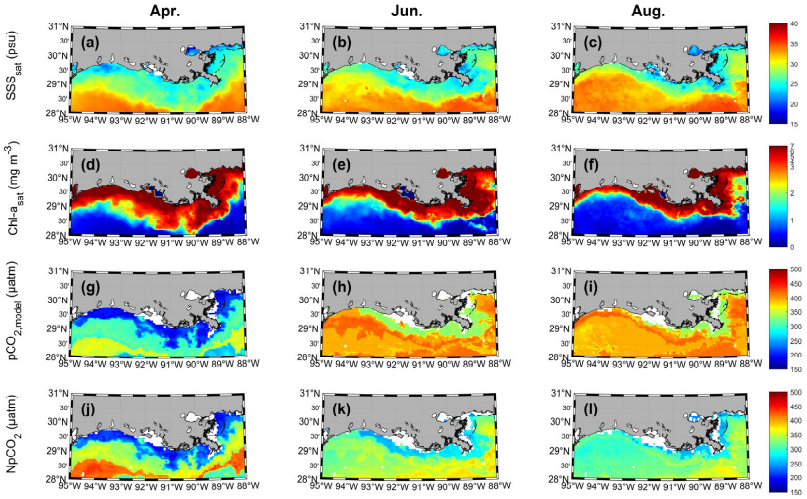

Figure 5. The spring-summer climatology of (a, b, c) satellite-derived sea surface salinity (SSS_{sat}); (d, e, f) satellite-derived chlorophyll a (Chl-a_{sat}); (g, h, i) sea surface pCO_2 from the season-specific random forest model ($pCO_{2,model}$); (j, k, l) non-thermal pCO_2 (NpCO_2) in April (the first column), June (the second column), and August (the third column).

The regional monthly averages of spring and summer across different years capture not only seasonal variations but also interannual differences (Fig. 6). The positive correlation between TN load and Chl-a_{sat} in both spring and summer shows the stimulation of phytoplankton growth by riverine nutrients (Fig. 6a). High Chl-a_{sat} corresponds to enhanced biological CO_2 uptake, resulting in negative correlations between Chl-a_{sat} and NpCO_2 (Fig. 6b). While rising SST in spring and summer tends to increase pCO_2, the concurrent biologically mediated reduction partially counteracts the thermal forcing, and stronger biological uptake under higher riverine nutrient input leads to relatively lower pCO_2 (Fig. 5). The seasonal amplitude of SST in the nGOM is relatively stable (annual amplitude of 25.1±1.5 °C), but river discharge and nutrient transport exhibit considerable interannual fluctuation. When focusing on interannual variability, analysis of spring-summer averages across different years reveals that in years with higher river discharge, the greater nutrient input exerts a stronger stimulatory effect on phytoplankton productivity (Fig. 6c). The higher discharge also enhances stratification, favoring the accumulation of biological signals and thus leading to lower pCO_2 (Fig. 6d). Consequently, year-to-year differences in riverine freshwater and nutrient inputs dominantly control the interannual variability of spring-summer pCO_2 in the nGOM.

https://doi.org/10.5194/egusphere-2026-3034
Preprint. Discussion started: 11 June 2026

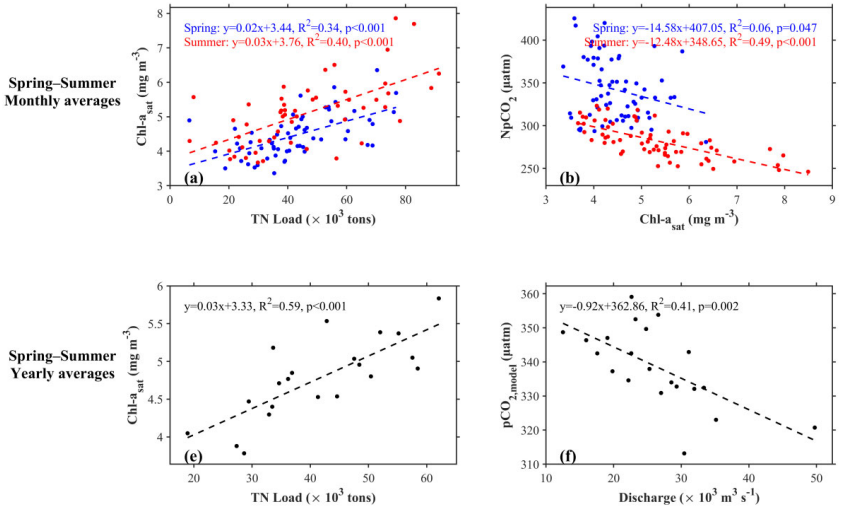

Figure 6. Relationship between regional spring-summer monthly averages of (a) Mississippi River total nitrogen (TN) load and satellite-derived chlorophyll a (Chl-a_{sat}); (b) Chl-a_{sat} and non-thermal driven change in pCO_2 (NpCO_2). A one-month time lag is applied to Chl-a_{sat} and NpCO_2 relative to riverine TN load in panels (a) to account for the delayed biological response (e.g., March TN load paired with April Chl-a_{sat}). Relationship between regional spring-summer yearly averages of (c) TN load vs. Chl-a_{sat}; (d) river discharge vs. sea surface pCO_2 from the season-specific random forest model ($pCO_{2,model}$) over the period of 2003 to 2024.

Vertical mixing effect in autumn and winter: In contrast to spring and summer when stratification limits vertical mixing, surface cooling (Fig. 4a, Fig. 7a-c) and increased wind speeds (Fig. 4h) in autumn and winter promote vertical mixing (Fig. 7d-f, Fig. 8a). Concurrently, the marked decline in Chl-a (Fig. 4d) during autumn and winter reduces biological activity, thereby diminishing the biological influence. As a result, the dominant non-thermal mechanism shifts from biological uptake in spring and summer to vertical mixing in autumn and winter. Enhanced vertical mixing brings CO_2-rich deeper water with higher concentration of dissolved inorganic carbon (DIC) to the surface, leading to an increase in NpCO_2 (Fig. 4f; Fig. 7j-l). However, the mixing scheme differs between the inner shelf where summer bottom hypoxia and acidification occur and offshore region. On the inner shelf, the maximum mixed layer depth (MLD) is limited by the shallow bottom. Mixing entrains bottom water that has accumulated CO_2 during summer stratification, thereby raising surface NpCO_2. In offshore region where water depth is greater, the MLD deepens

https://doi.org/10.5194/egusphere-2026-3034
Preprint. Discussion started: 11 June 2026

progressively in autumn and winter reaching ~80 m, and mixes surface water with subsurface water containing higher DIC. The inner shelf, under the influence of riverine nutrients, experiences higher productivity and therefore accumulates a larger signal of respired CO_2 from organic matter decomposition compared to the offshore subsurface water. Consequently, mixing with inner-shelf bottom water has a more pronounced effect on increasing surface NpCO_2 than mixing with offshore subsurface water. As a result, the slope of the relationship between NpCO_2 and MLD is steeper on the inner shelf than in the offshore region (Fig. 8b).

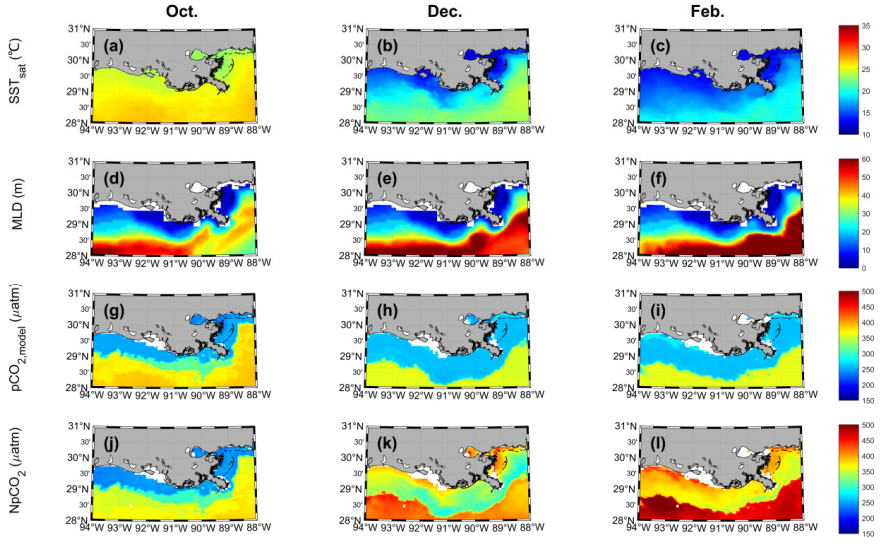

Figure 7. The autumn-winter climatology of (a, b, c) satellite-derived sea surface temperature (SST_{sat}); (d, e, f) mixed layer depth (MLD); (g, h, i) sea surface pCO_2 from the season-specific random forest model ($pCO_{2,model}$); (j, k, l) non-thermal pCO_2 (NpCO_2) in October (the first column), December (the second column), and February (the third column).

https://doi.org/10.5194/egusphere-2026-3034
Preprint. Discussion started: 11 June 2026

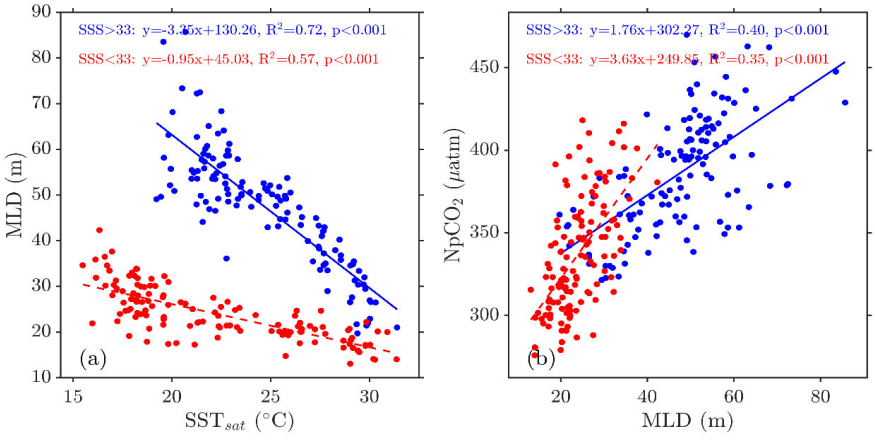

Figure 8. Relationship between regional monthly averages of (a) satellite-derived sea surface temperature (SST_{sat}) and mixed layer depth (MLD); (b) MLD and non-thermal driven change in pCO_2 ($NpCO_2$) on the inner shelf (red, sea surface salinity < 33) and in the offshore region (blue, sea surface salinity > 33) in autumn and winter months (2003 to 2024).

3.4 Decadal variability

3.4.1 Decadal trends

Linear regression of regional monthly averages from 2003 to 2024 reveals that SST in the nGOM increased at a rate of 0.05 ± 0.01 °C yr^{-1} (Fig. 9a), consistent with the previous remote sensing-based assessment [*Li et al.*, 2022]. Corresponding to the long-term increasing trend in river discharge (Fig. 9b), SSS exhibits a weak decreasing trend (Fig. 9c). Although freshwater input has increased from 2003 to 2024, nutrient management and control implemented in the Mississippi River basin have resulted in no statistically significant change in riverine TN load over recent decades (Fig. 9d) [*Howarth et al.*, 2011; *McIsaac et al.*, 2001]. Nevertheless, Chl-a in the nGOM shows a long-term increasing trend (0.04 ± 0.01 mg m^{-3} yr^{-1}, Fig. 9e), consistent with previous studies [*Li et al.*, 2022; *Muller-Karger et al.*, 2015]. The driver of this Chl-a increase is likely the extension of the phytoplankton growing season caused by rising SST, which provides a longer window for biomass accumulation [*Boyce et al.*, 2010; *Rabalais et al.*, 1996]. Other factors affecting Chl-a trend involve wind-induced Ekman suction, convective mixing during cold events,

https://doi.org/10.5194/egusphere-2026-3034
Preprint. Discussion started: 11 June 2026

coastal circulation, and mesoscale eddy activity [*Li et al.*, 2022].

In response to ocean warming, the thermally driven TpCO_2 exhibits an increasing trend (0.52 ± 0.17 µatm yr^{-1}, Fig. 9f). Meanwhile, the observed increase in Chl-a would be expected to inhibit the rise in sea surface pCO_2 through enhanced biological carbon fixation. Additionally, the winter warming-induced weakening of vertical mixing may reduce the entrainment of CO_2-rich deep water, leading to a decreasing trend in NpCO_2 (-0.25 ± 0.18 µatm yr^{-1}, Fig. 9f). Combining these opposing effects, sea surface pCO_2 shows a slight increasing trend at a rate of 0.50 ± 0.20 µatm yr^{-1} (Fig. 9g), similar to the long-term change rate of 0.08 ± 1.66 µatm yr^{-1} estimated for the northcentral Gulf of Mexico from the SOCAT dataset (1996–2017) [*Kealoha et al.*, 2020]. This suggests that the positive effect of rising SST outweighs the negative effect of biological carbon fixation and weakening vertical mixing. The long-term increase rate of sea surface pCO_2 is much lower than that of atmospheric pCO_2 (2.13 ± 0.04 µatm yr^{-1}, Figure 9g), driving a significant decline in the air-sea pCO_2 difference at a rate of -1.63 ± 0.20 µatm yr^{-1}. That is, the partial pressure gradient continues to shift toward enhanced ocean uptake of atmospheric CO_2. With no significant long-term shift in wind speed (Fig. 9h), the increasing air-sea pCO_2 gradient leads to a strengthening oceanic CO_2 sink, with FCO_2 decreasing (more negative) at a rate of -0.41 ± 0.06 mmol C m^{-2} d^{-1} yr^{-1} (Fig. 9i).

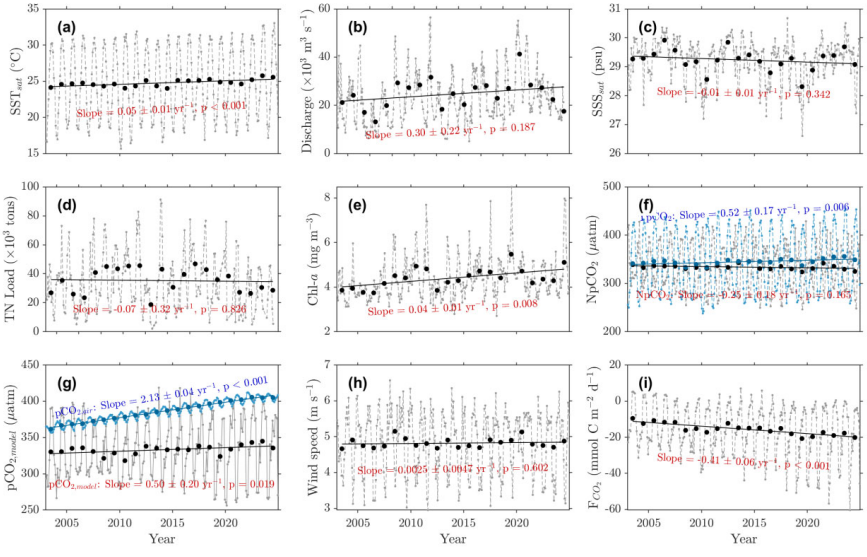

Figure 9. Long-term trends of (a) satellite-derived sea surface temperature (SST_{sat}); (b) Mississippi River discharge; (c) satellite-derived sea surface salinity (SSS_{sat}); (d) Mississippi

https://doi.org/10.5194/egusphere-2026-3034
Preprint. Discussion started: 11 June 2026

River total nitrogen (TN) load; (e) satellite-derived chlorophyll a (Chl-a_{sat}); (f) sea surface pCO_2 ($pCO_{2,model}$) and atmospheric pCO_2 ($pCO_{2,air}$); (g) air-sea pCO_2 difference (ΔpCO_2, seawater minus atmosphere); (h) wind speed; (i) sea-to-air CO_2 flux (F_{CO2}), where negative values refer to oceanic CO_2 uptake. Gray and black dots represent monthly and annual averages, respectively, for the northern Gulf of Mexico from 2003 to 2024. The solid black lines are linear regressions fitted to the annual averages.

3.4.2 The weakening westward Mississippi plume transport

Beyond the regionally averaged decadal trends, we further computed the decadal trend for each grid cell (Fig. 10). A prominent feature is that the western Texas-Louisiana shelf exhibits a significantly higher pCO_2 increasing rate (2.30 ± 1.00 µatm yr^{-1}, Fig. 10a). Previous study by *Kealoha et al.* [2020] also found that the northwestern Gulf of Mexico shows a higher long-term pCO_2 increasing rate (3.20 ± 1.47 µatm yr^{-1}) compared to the northcentral Gulf of Mexico (0.08 ± 1.66 µatm yr^{-1}). The temperature-normalized NpCO_2 also displays a high decadal increase rate in this region (Fig. 10b), indicating that ocean warming (Fig. 10c) alone is not responsible for the faster pCO_2 rise.

Our earlier analysis has shown that the high productivity of the river plume and its spatial distribution exert a strong influence on the spatiotemporal variability of pCO_2 in the nGOM (Section 3.3). On the western Texas-Louisiana shelf, numerical simulations indicate that the influence of Atchafalaya freshwater is mainly confined to nearshore regions within the 10 m isobath, whereas the westward extension of the Mississippi plume plays an important role in affecting waters on the shelf between the 10 m and 50 m isobaths [*Zhang et al.*, 2012a]. During the period 2003–2024, we identified a decreasing trend in the frequency of easterly (westward-blowing) wind (Fig. 10d), which would reduce the westward transport of Mississippi plume water. This is consistent with the observed increase in SSS on the western Texas-Louisiana shelf (Fig. 10e). Because Mississippi plume water is characterized by lower pCO_2 resulting from biological uptake and represents a nutrient delivery pathway to the western shelf, the reduced westward plume extension not only leads to less westward transport of low-pCO_2 water through physical mixing, but also decreases nutrient supply to the western shelf, thereby weakening biological CO_2 uptake there. We therefore infer that the wind-induced weakening of the westward transport of the Mississippi plume is a likely cause of the higher long-term pCO_2 increasing rate observed on the western shelf.

https://doi.org/10.5194/egusphere-2026-3034
Preprint. Discussion started: 11 June 2026

The observed wind-driven reduction in westward plume transport and its effect on pCO_2 trends add to a growing body of evidence that physical forcing (wind, currents) can strongly modulate the biological CO_2 sink in river-dominated margins. Similar mechanisms have been reported for the Changjiang River plume in the East China Sea, where wind shifts alter the dispersal of nutrient-rich water and thus coastal productivity [*Li et al.*, 2021; *Xu et al.*, 2024]. In contrast, the Amazon River plume, which extends far into the Atlantic, is more persistently influenced by large-scale ocean circulation than by local wind [*Kortzinger*, 2003]. Our findings highlight that even on a relatively narrow shelf like the Texas-Louisiana shelf, wind-driven changes in plume trajectory can produce significant spatial heterogeneity in long-term pCO_2 trends, with implications for the design of monitoring networks and for the interpretation of satellite-based pCO_2 products in river-influenced coastal zones.

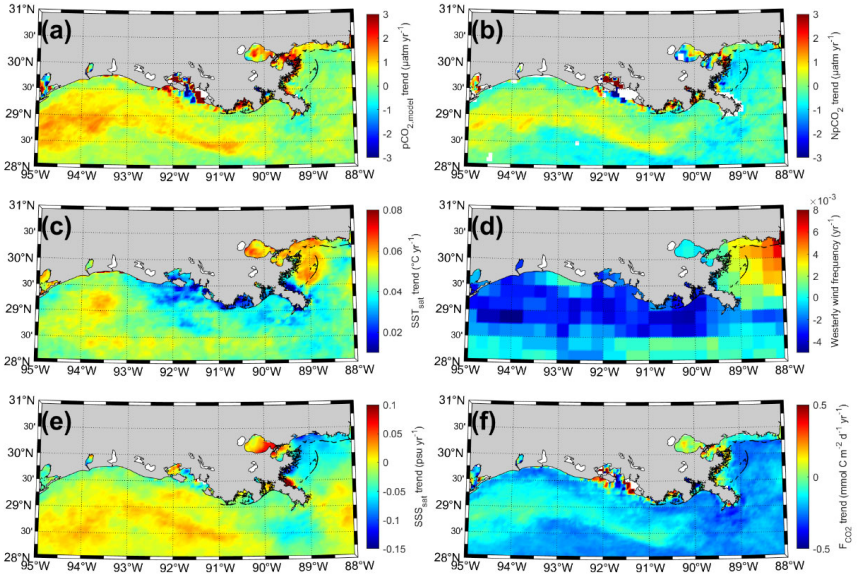

Figure 10. The gridded long-term changing rates of (a) sea surface pCO_2, (b) non-thermal driven change in pCO_2 ($NpCO_2$), (c) satellite-derived temperature (SST_{sat}), (d) probability of easterly wind, (e) sea surface salinity (SSS_{sat}), and (f) sea-to-air CO_2 flux (F_{CO2}), where negative values refer to oceanic CO_2 uptake in the northern Gulf of Mexico from 2003 to 2024.

https://doi.org/10.5194/egusphere-2026-3034
Preprint. Discussion started: 11 June 2026

4 Conclusions

Using a season-specific random forest model, we reconstructed a 22-year (2003–2024) high-resolution (4-km, 8-day) sea surface pCO_2 dataset for the nGOM. The trajectory of the productive Mississippi River plume largely determines the spatial distribution of sea surface pCO_2 in the nGOM. Biological CO_2 uptake fueled by riverine nutrients creates persistent low-pCO_2 water associated with the plume trajectory in the coastal region (SSS < 33), whereas the offshore high-salinity waters (SSS > 33) exhibit higher pCO_2 with smaller seasonal amplitude and weaker spatial heterogeneity. Seasonally, pCO_2 generally follows a temperature-driven pattern (high in summer, low in winter), but this thermal control is counteracted by two non-thermal processes: biological drawdown in spring and summer, and vertical mixing with CO_2-rich deep water during autumn and winter. Interannual variations in river discharge and nutrient loading dominate pCO_2 variability in the river-influenced coastal zone, with higher discharge leading to lower pCO_2 due to enhanced biological uptake. On a decadal timescale, sea surface pCO_2 increased at 0.50 μatm yr^{-1} accompanied by rising Chl-a in coastal regions. This increase is significantly slower than the atmospheric CO_2 rise (2.13 μatm yr^{-1}), leading to an enhanced ocean CO_2 sink with sea-to-air CO_2 flux becoming more negative at a rate of −0.41 mmol C m^{-2} d^{-1} yr^{-1}. Moreover, a weakening of easterly winds over 2003–2024 has reduced the westward transport of the Mississippi River plume, causing a higher pCO_2 increasing rate on the western Texas-Louisiana shelf. These findings provide critical constraints for regional carbon budgeting and highlight the complex interplay among riverine inputs, biological productivity, vertical mixing, wind-driven circulation, and atmospheric CO_2 forcing in shaping the coastal carbon sink.

Acknowledgments

This study was supported by National Natural Science Foundation of China (Grant 42376040).

Author contributions

Zong-Pei Jiang: Conceptualization, Methodology, Validation, Formal Analysis, Writing-Original

https://doi.org/10.5194/egusphere-2026-3034
Preprint. Discussion started: 11 June 2026

Draft, Writing-Review & Editing, Supervision, Funding Acquisition.

Fengqin Chen: Methodology, Software, Validation, Formal Analysis, Data Curation, Writing-Original Draft, Writing-Review & Editing, Visualization.

Wenzhao Liang: Methodology, Resources, Writing-Review & Editing.

Kailang Ma: Methodology, Data Curation, Formal Analysis, Writing-Review & Editing.

Chenfeng Le: Methodology, Resources, Writing-Review & Editing.

Yiwen Pan: Resources, Writing-Review & Editing, Funding Acquisition.

Wei-Jun Cai: Conceptualization, Methodology, Writing-Review & Editing, Resources, Supervision.

Code and data availability

The reconstructed pCO_2 data by the study are available at https://doi.org/10.5281/zenodo.20238487.

Competing interests

The authors declare there are no conflicts of interest for this manuscript.

Reference

Bauer, J. E., W. J. Cai, P. A. Raymond, T. S. Bianchi, C. S. Hopkinson, and P. A. G. Regnier (2013), The changing carbon cycle of the coastal ocean, *Nature*, *504*(7478), 61-70, doi:10.1038/nature12857.

Boyce, D. G., M. R. Lewis, and B. Worm (2010), Global phytoplankton decline over the past century, *Nature*, *466*(7306), 591-596, doi:10.1038/nature09268.

Cai, W. J., et al. (2011), Acidification of subsurface coastal waters enhanced by eutrophication, *Nature Geoscience*, *4*(11), 766-770, doi:10.1038/NGEO1297.

Chen, C.-T. A., and A. V. Borges (2009), Reconciling opposing views on carbon cycling in the coastal ocean: Continental shelves as sinks and near-shore ecosystems as sources of atmospheric CO_2, *Deep Sea Research Part II: Topical Studies in Oceanography*, *56*(8-10), 578-590, doi:10.1016/j.dsr2.2009.01.001.

Chen, S., C. Hu, B. Barnes, R. Wanninkhof, W.-J. Cai, L. Barbero, and D. Pierrot (2019), A machine learning approach to estimate surface ocean pCO_2 from satellite measurements, *Remote Sens. Environ.*, *228*, 203-226, doi:10.1016/j.rse.2019.04.019.

Chen, S., C. Hu, W.-J. Cai, and B. Yang (2017), Estimating surface pCO_2 in the northern Gulf of Mexico: Which remote sensing model to use?, *Cont. Shelf Res.*, *151*, 94-110, doi:10.1016/j.csr.2017.10.013.

https://doi.org/10.5194/egusphere-2026-3034
Preprint. Discussion started: 11 June 2026

Dai, M., et al. (2022), Carbon fluxes in the coastal ocean: Synthesis, boundary processes, and future trends, *Annu. Rev. Earth Planet. Sci.*, *50*, 593-626, doi:10.1146/annurev-earth-032320-090746.

Duan, X., P. Yin, X. He, B. Chen, K. Cao, and G. Tong (2025), Unraveling nonlinear interactions: A DPSIR-based conceptual model for synergistic impacts of climate change and human activities on coastal blue carbon ecosystems, *Global Change Biol.*, *31*(8), e70432, doi:https://doi.org/10.1111/gcb.70432.

Fichot, C. G., S. E. Lohrenz, and R. Benner (2014), Pulsed, cross-shelf export of terrigenous dissolved organic carbon to the Gulf of Mexico, *Journal of Geophysical Research: Oceans*, *119*(2), 1176-1194.

Gattuso, J.-P., M. Frankignoulle, and R. Wollast (1998), Carbon and carbonate metabolism in coastal aquatic ecosystems, *Annu. Rev. Ecol. Evol. Syst.*, *29*, 405-434.

Howarth, R., F. Chan, D. J. Conley, J. Garnier, S. C. Doney, R. Marino, and G. Billen (2011), Coupled biogeochemical cycles: eutrophication and hypoxia in temperate estuaries and coastal marine ecosystems, *Frontiers in Ecology and the Environment*, *9*(1), 18-26, doi:10.1890/100008.

Huang, W. J., W. J. Cai, R. M. Castelao, Y. C. Wang, and S. E. Lohrenz (2013), Effects of a wind-driven cross-shelf large river plume on biological production and CO_2 uptake on the Gulf of Mexico during spring, *Limnol. Oceanogr.*, *58*(5), 1727-1735, doi:10.4319/lo.2013.58.5.1727.

Huang, W. J., W. J. Cai, Y. C. Wang, S. E. Lohrenz, and M. C. Murrell (2015), The carbon dioxide system on the Mississippi River-dominated continental shelf in the northern Gulf of Mexico: 1. Distribution and air-sea CO_2 flux, *J. Geophys. Res.*, *120*(3), 1429-1445, doi:10.1002/2014JC010498.

Jiang, Z.-P., W.-J. Cai, B. Chen, K. Wang, C. Han, B. J. Roberts, N. Hussain, and Q. Li (2019a), Physical and biogeochemical controls on pH dynamics in the northern Gulf of Mexico during summer hypoxia, *Journal of Geophysical Research: Oceans*, *124*, JC015140, doi:10.1029/2019jc015140.

Jiang, Z.-P., C. Qin, Y. Pan, C. Le, N. Rabalais, R. E. Turner, K. Fennel, K. Wang, and W.-J. Cai (2024), Multi-Decadal Coastal Acidification in the Northern Gulf of Mexico Driven by Climate Change and Eutrophication, *Geophys. Res. Lett.*, *51*(5), e2023GL106300, doi:10.1029/2023GL106300.

Jiang, Z.-P., Y. Tong, M. Tong, J. Yuan, Q. Cao, and Y. Pan (2021), The effects of suspended particulate matter, nutrient, and salinity on the growth of *Amphidinium carterae* under estuary environmental conditions, *Frontiers in Marine Science*, *8*(887), doi:10.3389/fmars.2021.690764.

Jiang, Z. P., et al. (2019b), Spring net community production and its coupling with the CO_2 dynamics in the surface water of the northern Gulf of Mexico, *Biogeosciences*, *16*(18), 3507-3525, doi:10.5194/bg-16-3507-2019.

Kealoha, A. K., K. E. F. Shamberger, S. F. DiMarco, K. M. Thyng, R. D. Hetland, D. P. Manzello, N. C. Slowey, and I. C. Enochs (2020), Surface Water CO_2 variability in the Gulf of Mexico (1996–2017), *Scientific Reports*, *10*(1), 12279, doi:10.1038/s41598-020-68924-0.

Kortzinger, A. (2003), A significant CO_2 sink in the tropical Atlantic Ocean associated with the

https://doi.org/10.5194/egusphere-2026-3034
Preprint. Discussion started: 11 June 2026

Amazon River plume, *Geophys. Res. Lett.*

Laruelle, G., W.-J. Cai, X. Hu, N. Gruber, F. Mackenzie, and P. Regnier (2018), Continental shelves as a variable but increasing global sink for atmospheric carbon dioxide, *Nature Communications*, *9*, doi:10.1038/s41467-017-02738-z.

Laurent, A., K. Fennel, W.-J. Cai, W.-J. Huang, L. Barbero, and R. Wanninkhof (2017), Eutrophication-induced acidification of coastal waters in the northern Gulf of Mexico: insights into origin and processes from a coupled physical-biogeochemical model, *Geophys. Res. Lett.*, *44*, doi:10.1002/2016GL071881.

Le, C., Y. Gao, W.-J. Cai, J. C. Lehrter, Y. Bai, and Z.-P. Jiang (2019), Estimating summer sea surface pCO2 on a river-dominated continental shelf using a satellite-based semi-mechanistic model, *Remote Sensing of Environment*, *225*, 115-126, doi:10.1016/j.rse.2019.02.023.

Li, D., X. Ni, K. Wang, D. Zeng, B. Wang, H. Jin, H. Li, F. Zhou, D. Huang, and J. Chen (2021), Biological CO_2 uptake and upwelling regulate the air-sea CO_2 flux in the Changjiang Plume under south winds in summer, *Frontiers in Marine Science*, *8-2021*, doi:10.3389/fmars.2021.709783.

Li, G., Z. Wang, and B. Wang (2022), Multidecade trends of sea surface temperature, chlorophyll-a concentration, and ocean eddies in the Gulf of Mexico, *Remote Sensing*, *14*(15), 3754.

Lohrenz, S., W.-J. Cai, S. Chakraborty, W.-J. Huang, X. Guo, R. He, Z. Xue, K. Fennel, S. Howden, and H. Tian (2018), Satellite estimation of coastal pCO_2 and air-sea flux of carbon dioxide in the northern Gulf of Mexico, *Remote Sens. Environ.*, *207*, doi:10.1016/j.rse.2017.12.039.

McIsaac, G. F., M. B. David, G. Z. Gertner, and D. A. Goolsby (2001), Nitrate flux in the Mississippi River, *Nature*, *414*(6860), 166-167, doi:10.1038/35102672.

Muller-Karger, F. E., et al. (2015), Natural variability of surface oceanographic conditions in the offshore Gulf of Mexico, *Prog. Oceanogr.*, *134*, 54-76, doi:10.1016/j.pocean.2014.12.007.

Muller-Karger, F. E., R. Varela, R. Thunell, R. Luerssen, C. Hu, and J. J. Walsh (2005), The importance of continental margins in the global carbon cycle, *Geophys. Res. Lett.*, *32*(1), doi:10.1029/2004GL021346.

Rabalais, N. N., R. E. Turner, D. JustiĆ, Q. Dortch, W. J. Wiseman, and B. K. Sen Gupta (1996), Nutrient changes in the Mississippi River and system responses on the adjacent continental shelf, *Estuaries*, *19*(2), 386-407, doi:10.2307/1352458.

Rabalais, N. N., R. E. Turner, and W. J. Wiseman (2002), Gulf of Mexico hypoxia, aka "The dead zone", *Annu. Rev. Ecol. Syst.*, *33*, 235-263, doi:10.1146/annurev.ecolsys.33.010802.150513.

Roobaert, A., L. Resplandy, G. G. Laruelle, E. H. Liao, and P. Regnier (2024), Unraveling the physical and biological controls of the global coastal CO_2 sink, *Global Biogeochem. Cycles*, *38*(3), doi:10.1029/2023GB007799.

Schiller, R. V., V. H. Kourafalou, P. Hogan, and N. D. Walker (2011), The dynamics of the Mississippi River plume: Impact of topography, wind and offshore forcing on the fate of plume waters, *J. Geophys. Res.*, *116*, doi:10.1029/2010jc006883.

https://doi.org/10.5194/egusphere-2026-3034
Preprint. Discussion started: 11 June 2026

Takahashi, T., J. Olafsson, J. G. Goddard, D. W. Chipman, and S. C. Sutherland (1993), Seasonal variation of CO_2 and nutrients in the high-latitude surface oceans: A comparative study, *Global Biogeochem. Cycles*, *7*(4), 843-878, doi:10.1029/93GB02263.

Turner, R. E., N. N. Rabalais, and D. Justic (2006), Predicting summer hypoxia in the northern Gulf of Mexico: Riverine N, P, and Si loading, *Mar Pollut Bull*, *52*(2), 139-148, doi:10.1016/j.marpolbul.2005.08.012.

Walker, N. D. (1996), Satellite assessment of Mississippi River plume variability: Causes and predictability, *Remote Sens. Environ.*, *58*(1), 21-35, doi:10.1016/0034-4257(95)00259-6.

Walsh, J. J. (1991), Importance of continental margins in the marine biogeochemical cycling of carbon and nitrogen, *Nature*, *350*(6313), 53-55, doi:10.1038/350053a0.

Wanninkhof, R. (2014), Relationship between wind speed and gas exchange over the ocean revisited, *Limnol. Oceanogr. Methods*, *12*(JUN), 351-362, doi:10.4319/lom.2014.12.351.

Wei, H., Y. Deng, U. P. K. Epa, B. D. Belle, B. Sharma, H. Zhang, and H. Sa (2025), Scientific advances and future trends in ocean carbon sink: an interdisciplinary review, *Frontiers in Marine Science*, *Volume 12 - 2025*, doi:10.3389/fmars.2025.1658207.

Weiss, R. F. (1974), Carbon dioxide in water and seawater: the solubility of a non-ideal gas, *Mar. Chem.*, *2*, 203-215, doi:10.1016/0304-4203(74)90015-2.

Wu, Z., H. Wang, E. Liao, C. Hu, K. Edwing, X.-H. Yan, and W.-J. Cai (2024), Air-sea CO2 flux in the Gulf of Mexico from observations and multiple machine-learning data products, *Prog. Oceanogr.*, *223*, 103244, doi:10.1016/j.pocean.2024.103244.

Xu, M., Y. Wang, Z. Feng, and H. Wu (2024), Rapid variations of phytoplankton blooms and their dynamics off the Changjiang River Estuary, *Frontiers in Marine Science*, *Volume 11 - 2024*, doi:10.3389/fmars.2024.1345940.

Zeebe, R. E., Wolf-Gladrow, D.A. (2001), CO_2 in Seawater: Equilibrium, Kinetics, Isotopes, *Elsevier Oceanography Series*, *65*, 346.

Zhang, X., R. D. Hetland, M. Marta-Almeida, and S. F. DiMarco (2012a), A numerical investigation of the Mississippi and Atchafalaya freshwater transport, filling and flushing times on the Texas-Louisiana Shelf, *Journal of Geophysical Research: Oceans*, *117*(C11), doi:10.1029/2012jc008108.

Zhang, X. Q., R. D. Hetland, M. Marta-Almeida, and S. F. DiMarco (2012b), A numerical investigation of the Mississippi and Atchafalaya freshwater transport, filling and flushing times on the Texas-Louisiana Shelf, *J. Geophys. Res.*, *117*, doi:10.1029/2012jc008108.